GeoScienceWorld
Lithosphere
Volume 2023, Article ID lithosphere_2023_126, 16 pages
https://doi.org/10.2113/2023/lithosphere_2023_126

Lithosphere

Research Article

Behavior of Platinum-Group Elements during Hydrous Metamorphism: Constraints from Awaruite (Ni_3Fe) Mineralization

Anton Kutyrev[1], **Vadim S. Kamenetsky**[2,3], **Alkiviadis Kontonikas-Charos**[4], **Dmitry P. Savelyev**[5], **Tamara Yu. Yakich**[6], **Ivan A. Belousov**[7], **Elena I. Sandimirova**[8] and **Svetlana V. Moskaleva**[9]

[1]*Department of Earth Sciences, University of Oregon, Eugene, Oregon, 97403, USA*
[2]*Center of Deep Sea Research, Institute of Oceanology, Chinese Academy of Sciences, Qingdao 266071, P. R. China*
[3]*Laboratory of Mineralogy, Institute of Volcanology and Seismology FEB RAS, Petropavlovsk-Kamchatsky, 683006, Russia*
[4]*School of Earth and Atmospheric Sciences, Queensland University of Technology, Brisbane, Queensland 4001, Australia*
[5]*Laboratory of Petrology and Geochemistry, Institute of Volcanology and Seismology FEB RAS, Petropavlovsk-Kamchatsky, 683006, Russia*
[6]*Tomsk Polytechnic University, Tomsk, Russia*
[7]*Center for Ore Deposit and Earth Sciences (CODES), School of Natural Sciences, University of Tasmania, Hobart, TAS 7001, Australia*
[8]*Geothermal Laboratory, Institute of Volcanology and Seismology, Petropavlovsk-Kamchatksy, 683006, Russia*
[9]*Laboratory of Volcanogenic Ore Genesis, Institute of Volcanology and Seismology, Petropavlovsk-Kamchatsky, 683006, Russia*

Correspondence should be addressed to Anton Kutyrev; anton.v.kutyrev@gmail.com

Received 1 March 2023; Accepted 14 September 2023; Published 17 October 2023

Academic Editor: Aleksandr S. Stepanov

Natural Fe-Ni alloys are common in meteorites and, presumably, the Earth's core, where they host significant platinum-group elements (PGE). However, little is known on PGE concentrations in hydrothermal or metamorphic Fe-Ni alloys (i.e., awaruite Ni_3Fe) from terrestrial rocks. In this work, we examine the geochemistry of awaruite and related minerals from several placer deposits sourced from the suprasubduction ophiolitic (Kamchatsky Mys, Karaginsky Island, and Mamet) and Ural-Alaskan (Galmoenan) complexes of Kamchatka and the Koryak Highlands (Far East Russia) in order to assess the abundance of PGE in awaruite and constrain their mobility under metamorphic and hydrothermal conditions. Studied awaruite from ophiolitic and Ural-Alaskan type complexes formed via desulfurization of pentlandite during serpentinization. Three groups of platinum-group minerals (PGMs) are associated with awaruite from Kamchatsky Mys: (1) Pt-Fe alloys such as ferronickelplatinum (Pt_2FeNi) or unnamed Ni_2FePt alloys; (2) Os-Ir-Ru alloys of various composition; (3) Pd-Sb minerals which form together with serpentine during hydrothermal alteration. Despite the abundance of PGM inclusions, no significant PGE concentrations were measured in awaruite from the Kamchatsky Mys, Karaginsky Island, or Mamet ophiolites. In contrast, pentlandite relicts in awaruite from placers related to the Galmoenan Ural-Alaskan type complex contain exceptionally high, previously unreported, Os (up to 540 ppm). Awaruite that forms on behalf of this pentlandite does not show any significant Os enrichment. Rare Galmoenan awaruite analyses yield up to 3 ppm Pd. The new data are not in complete accordance with previous studies that reported relatively high (up to first 10 ppm) PGE content in awaruite. We attribute this to low PGE concentration in precursor sulfides and preferential partitioning of PGE into discrete secondary PGM within awaruite. Nevertheless, abundant inclusions of secondary PGM in awaruite provide evidence of PGE mobility during metamorphic and hydrothermal alteration of ultramafic rocks.

1. Introduction

Primarily sourced from layered mafic intrusions, platinum-group elements (PGE: Os, Ir, Ru, Rh, Pt, and Pd) are typically found within chromitites and/or Ni-, Co-, and Cu-rich sulfide deposits [1, 2], placers associated with Ural-Alaskan and Aldan type complexes [3, 4], and ophiolitic peridotites [5]. In each of these occurrences, the majority of researchers propose magmatic origins for platinum-group minerals (PGMs). Although magmatic PGMs, such as native metals and alloys, are generally considered to be resistant to postmagmatic processes, recent studies have shown that the effects of alteration in the crust cannot be discounted [6–9].

Serpentinization is the most common type of alteration affecting PGE- and PGM-bearing peridotites in the crust and involves the replacement of olivine and pyroxene by serpentine minerals and magnetite via aqueous fluid-rock interaction [10–12]. This is a redox reaction in which one compound in the intermediate oxidation state converts to two compounds, one of higher and one of lower oxidation states. Subsequently, it may stabilize native phases and alloys including awaruite (Ni_2Fe–Ni_3Fe), wairauite (FeCo), and native Fe at the expense of Fe-bearing base metal sulfides (BMSs) and olivine [13, 14]. The most abundant of these alloys is awaruite, which occurs in most ophiolitic peridotites worldwide [15–18], as well as in other peridotites from different geodynamic settings [19]. Given the siderophile nature of PGE and evidence for their co-occurrence with secondary base metal alloys [9, 20], we hypothesize that awaruite may act as a major repository for PGE, particularly during hydrothermal and metamorphic processes.

Such assertions, however, are limited by the scarcity and variability of available data on PGE contents in awaruite from ophiolitic peridotites. Augé et al. [21] reported SIMS analyses of up to 1210 ppm Pt in awaruite, while Lawley et al. [22] measured 10–20 ppm Os, 0.1–7 ppm Ir, and up to 50 ppm ΣPGE in ophiolitic awaruite using LA-ICP-MS. In contrast, González-Jiménez et al. [23] found significantly lower PGE in ophiolitic awaruite, with the highest concentrations only reaching 6.9 ppm Rh and 2.5 ppm Pd. Scott and Jackson [24] reported some Pt and Pd admixtures in awaruite from Jamaican peridotites. Moreover, as only ophiolitic awaruite has been studied thus far, other types of ultramafic complexes such as Ural-Alaskan might provide additional insight and useful comparison.

Here, we examine the geochemistry of awaruite and related minerals from several placer deposits sourced from the suprasubduction ophiolitic and Ural-Alaskan complexes of the Kamchatka and Koryak Highlands (Far East Russia). The overarching goal of this study is to assess the behavior of PGE during the formation of awaruite, that is, under conditions corresponding to serpentinization and other metamorphic/hydrothermal processes.

2. Geological Background

2.1. Ophiolitic Peridotites. Ophiolitic peridotites in the study area comprise the following complexes: Kamchatsky Mys ophiolite (Mt. Soldatskaya ultramafic complex, Figure 1(a)), Mamet complex (part of the larger Kuyul complex) on the Mametchinsky peninsula (Figure 1(b)), and the Karaginsky complex on Karaginsky island (Figure 1(c)). All are composed of spinel harzburgite with subordinate dunite and less abundant peridotites (i.e., lherzolite, clinopyroxenites, and websterites).

The Kamchatsky Mys (also referred to as "Cape Kamchatsky") ophiolite complex in the easternmost Kamchatka Peninsula is renowned for its present-day tectonic position at the junction of the Kuril-Kamchatka arc, Aleutian arc, and Hawaiian-Emperor's seamount chain [25]. It comprises all members of classical ophiolite peridotites, gabbro, and basalts. Peridotites are interpreted to have formed in suprasubduction settings [26] or as components of an accretionary prism initially sourced from abyssal peridotites of the mid-ocean ridge [27]. Some researchers noted the heterogeneous nature of the complex, that is, the presence of both restitic peridotites of abyssal and suprasubduction types, as well as suprasubduction cumulates [28]. Its age is estimated between 112 and 92 Ma based on radiolarians associated with the Smagina Formation [29, 30]. According to some studies, basalts and volcano-sedimentary deposits of the Smagina Formation were formed under the influence of a Hawaiian hotspot in the oceanic spreading center [31–33]. The Kamchatsky Mys ophiolite is the source for the PGM placer of the Olkhovaya-1 river [34]. The samples were collected in the River Belaya canyon, where it flows through the outcrops of peridotites.

The Karaginsky ophiolite is located on Karaginsky island, approximately 50 km east of Kamchatka (Figure 1(b)), and is part of the late Cretaceous Olyutorsky (also known as "Achayvayam-Valaginsky") arc terrane. The Karaginsky peridotites likely formed in the mid-oceanic ridge and subsequently underwent metasomatic alteration in the suprasubduction setting [35].

The Mamet complex is a part of the larger Kuyul ophiolite located at the northern part of Penzhina bay (Figure 1(c)). It comprises harzburgitic restites and basal wehrlite-gabbro cumulate layers and likely interacted with primitive arc magmas [36]. The samples were collected in small creeks flowing in the serpentinized peridotites (Figure 1(c)).

2.2. Galmoenan Ural-Alaskan Type Complex. Known today as a prime example of Ural-Alaskan types, the Galmoenan complex was discovered in the 1960s and was initially thought to be part of an ophiolitic assemblage until later studies in the 1980s proved it to be a Ural-Alaskan type complex [37]. This gave grounds for Pt exploration and led to the discovery of unique placers that yielded >60 metric tons of Pt between 1994 and 2012 [38]. The complex is located in the Olyotursky arc terrane (Figure 1(d)). Like other Ural-Alaskan type complexes, it comprises arc

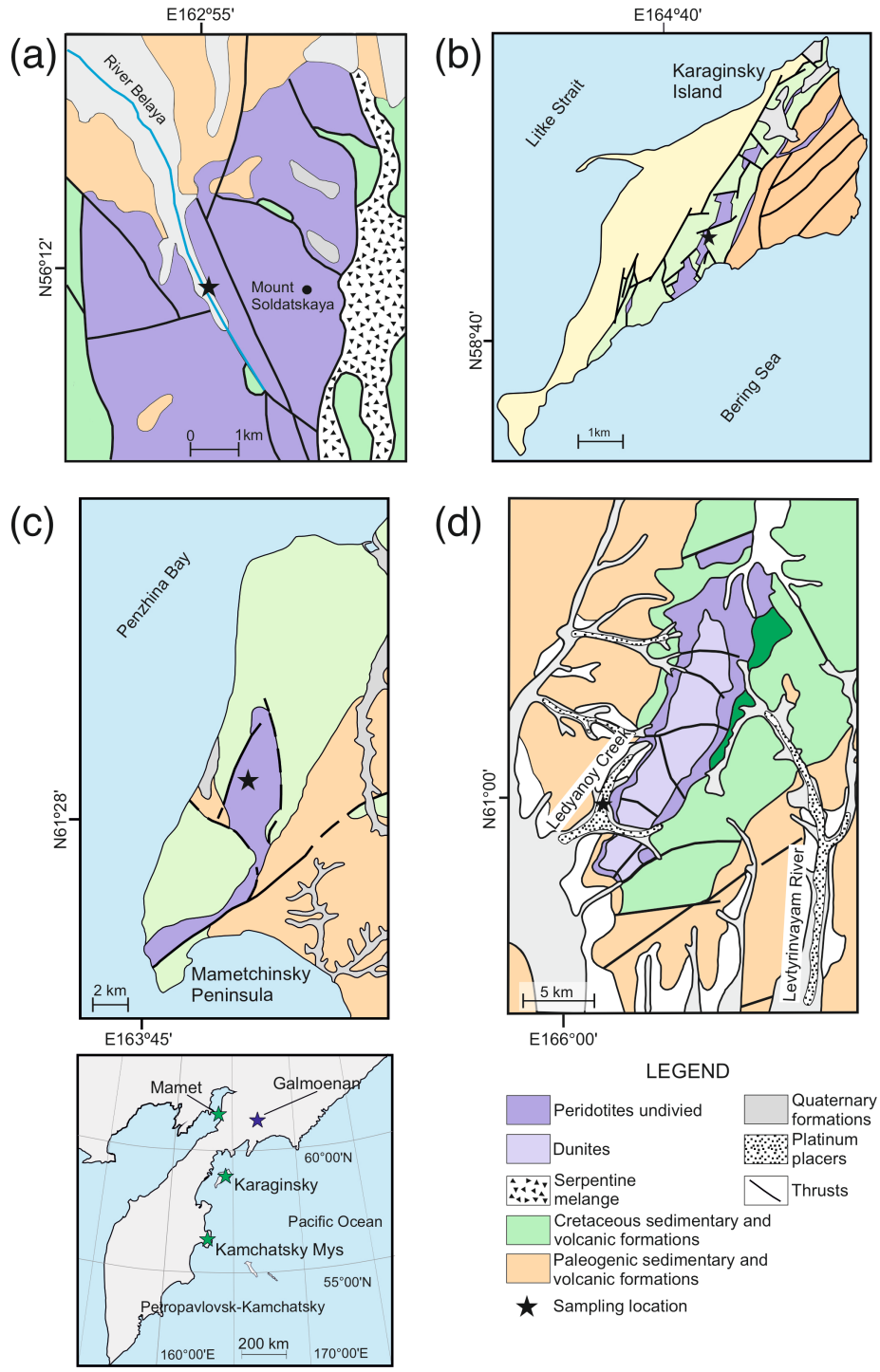

FIGURE 1: Geological maps of the studied complexes and sampling localities: (a) Kamchatksy Mys [76], (b) Karaginsky Island [36], (c) Mametchinsky Peninsula (modified after [77]), (d) Galmoenan (modified after [78]), and (e) position of the studied complexes within the Kamchatka region. Green stars represent ophiolitic peridotites, whereas the purple star is for the Ural-Alaskan type Galmoenan complex.

magma cumulates from the plumbing system of an arc volcano, subject to various recrystallization and alteration processes. Comprehensive reviews on Ural-Alaskan type complex structure, composition, and origin are available in References [3, 37, 39–41]. Studied samples were panned in the platinum placer of the Ledyanoy creek.

3. Sampling Strategy and Analytical Methods

Representative samples were obtained from creeks and rivers intersecting several ultramafic complexes of the Kamchatka Peninsula and adjacent Koryak Highlands during fieldwork spanning 1980–2020. Each sampling point

was located in a stream within the contour of the ultramafic body or within close proximity to ensure the origin of the awaruite. Rivers and tributaries were panned; concentrates of heavy minerals were examined in-field under a microscope to determine the most promising areas. These were then panned using large sluice boxes. The extracted heavy-mineral concentrates were sieved into four fractions: <0.1 mm, 0.1–0.25 mm, 0.25–0.5 mm, and >0.5 mm. Magnetic minerals from each fraction were separated using a very weak magnet. Since awaruite is more magnetic than magnetite, its proportion in the resulting concentrate was high. Grains with metallic luster were then hand-picked.

Approximately 300 grains from Kamchatsky Mys, 100 grains from Galmoenan and Mamet, and 10 grains from Karaginsky were studied by scanning electron microscopy to characterize their major element composition and locate PGM inclusions. A limited number of grains were analyzed by LA-ICP-MS: fifteen for Galmoenan, ten for the Mamet, and five for Kamchatsky Mys and Karaginsky Island. From these, seventy-seven total LA-ICP-MS analyses were carried out (including both awaruite, wairauite, and sulfide inclusions).

3.1. Electron Microscopy and EDS Analyses. The compositions of PGM were analyzed by energy-dispersive X-ray spectrometry using a Tescan VEGA-3 system equipped with an Oxford XMax80 EDS detector. A beam accelerating voltage of 20 kV, a 20-second count time, and 0.7 nA current intensity were used. The following analytical lines of X-ray spectra were used to detect elements: Mα lines—Pt, Os, and Ir; Lα lines—Ru, Rh, Pd, and As; and Kα lines—Fe, Cu, S, Ni, Al, Mg, Ca, V, Mn, Ti, Cr, and O. The following standards were used: pure metallic Pt, Os, Ir, Ru, Rh, and Pd for PGE, sanidine for Si, K, and Na, blue diopside for Ca, MgO for Mg, Al_2O_3 for Al, TiO_2 for Ti, $AlPO_4$ for P, V_2O_5 for V, rhodonite for Mn, FeS_2 for Fe and S, and pure metallic for Ni. The studied PGM inclusions in awaruite were too small for quantitative analysis; therefore, their compositions are not published, and EDS results are used for mineral identification purposes only.

3.2. LA-ICP-MS. In-situ LA-ICP-MS analyses were performed at the Center for Ore Deposit and Earth Sciences Analytical Laboratories, University of Tasmania, on an Applied Spectra/ASI RESOlution LR laser microprobe equipped with a Coherent Compex Pro ArF excimer laser with 193 nm wavelength and 20 ns pulsewidth and Laurin Technic S-155 cell and coupled to an Agilent 7700 quadrupole ICP MS. A beam size of 43 μm was used with a pulse rate of 5 Hz and laser beam fluence of 2.7 J/cm^2. Ablation was performed in a He atmosphere flowing at 0.35 L/min. The ablated aerosol was mixed with Ar (1.05 L/min) as a transport gas, before exiting the cell. Tuning was performed to minimize oxides (<0.15% ThO/Th) and maximize sensitivity for the mid- and high-mass isotopes. The following isotopes were measured: ^{34}S, ^{57}Fe, ^{59}Co, ^{60}Ni, ^{63}Cu, ^{65}Cu, ^{66}Zn, ^{99}Ru, ^{101}Ru, ^{103}Rh, ^{105}Pd, ^{106}Pd, ^{111}Cd, ^{125}Te, ^{185}Re, ^{189}Os, ^{193}Ir, ^{195}Pt, ^{197}Au, and ^{206}Pb. Dwell times were 5 ms for S, 10 ms for Fe, Co, Ni, Cu, Zn, and Pb, 20 ms for Cd, and 30 ms for all other elements, resulting in a total sweep time of 0.433 seconds. Analyses were performed in time-resolved mode with a total acquisition time of 90 seconds for each analysis, consisting of a 30 seconds background gas measurement and 60 seconds of ablation signal acquisition. Quantification was performed following the standard methods [42, 43] using LADR software [44]. Calibration involved STDGL3 [45], NiS3 [46], and Po724-T [47] reference materials all analyzed with 50 μm spot size. Instrumental drift was corrected by hourly analyses of reference materials across the analytical session. Fe was used as the internal standard element. Correction coefficients of 0.6 were applied to Zn and Cd concentrations consistent with previous work on sulfides when using STDGL2b2 and STDGL3 standards for quantification [45, 48]. Although ^{34}S was measured, preference was given to calculated composition due to significant Fe/S fractionation in different sulfides [49] and a need for matrix-matched quantification for precise measurement of sulfur by LA-ICP-MS. Instead, sulfides were calculated as monosulfides, while awaruite and wairauite were calculated as native metals with quantification involving normalization to 100 wt.% total. Measured sulfur is given only for analyses where calculated and measured sulfur values are drastically different.

Corrections for base metal-argide interferences are required for the quantification of Ru, Rh, and Pd by LA-ICP-MS techniques [50]. The analysis of magmatic sulfides has the potential to form ^{61}Ni^{40}Ar interferences on ^{101}Ru, ^{59}Co^{40}Ar on ^{99}Ru, ^{63}Cu^{40}Ar on ^{103}Rh, ^{65}Cu^{40}Ar on ^{105}Pd, and ^{66}Zn^{40}Ar on ^{106}Pd. For the quantification of Ru, Rh, and Pd, the extent of base metal-argide species production was determined by ablating lines on pure Ni, Cu, Zn, and Co metals in duplicates at the beginning and end of the session. All corrections were based on count rates and were done in LADR software. Contents of ^{106}Pd were also corrected for isobaric interference from ^{106}Cd, which was monitored by recording the signal on ^{111}Cd. In cases where concentrations measured on different Ru and Pd isotopes were showing similar results, averages were taken, whereas if they were significantly different, the isotope with less interference was chosen.

4. Results

4.1. Morphology of Awaruite and Wairauite Grains. Awaruite typically occurs as shiny, yellow, rounded metallic particles without any primary crystal morphology (Figures 2(a)–2(d)). They often form intergrowth textures with silicates, the latter of which may also be predominant in some grains (Figure 2(d)). Wairauite is rare; its distinct grains are only found in placers related to the Galmoenan and Mamet complexes. In the Mamet complex, they almost exclusively form perfect cubic crystals twinned by the fluorite law (Figures 2(e) and 2(f)).

4.2. Mineralogy and Petrography of Ophiolitic Awaruite. Awaruite from the Kamchatsky Mys ophiolites predominantly forms as an alteration product of pentlandite. Grains typically comprise a pentlandite core

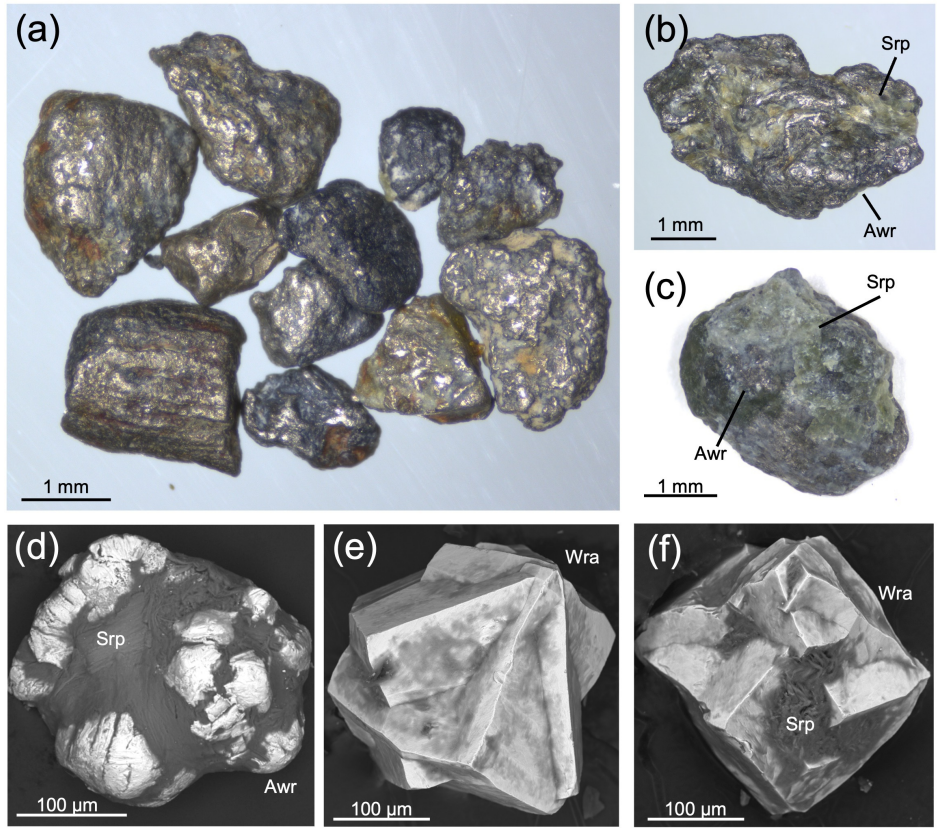

Figure 2: Grains of awaruite from Kamchatsky Mys (a–c), and back-scattered electron (BSE) images of awaruite (d) and wairauite (e and f) from Mamet. Awr – awaruite, Srp – serpentine, and Wra – wairauite.

surrounded by a replacement rim of awaruite (Figures 3(a) and 3(b)). Inclusions of BMS (pentlandite and/or heazlewoodite and pyrrhotite) are also observed within awaruite (Figure 3(c)). Another common occurrence is awaruite forming veins in pentlandite (Figure 3(d)) or as fine-grained awaruite-serpentine aggregates (Figure 3(e)). In most cases, sulfides also show minor alteration and replacement by iron oxides and hydroxides. Occasionally, awaruite coexists with droninoite (Figure 3(f)) and may form intergrowths with magnetite (Figure 3(g)). Native copper is abundant and generally forms anhedral aggregates toward the rims of awaruite grains (Figures 3(g) and 3(h)). Rare wairauite occurs as euhedral crystals within the awaruite-serpentine aggregates (Figure 3(i)). Their euhedral shape indicates that they likely crystallized in the presence of free space, which, together with their textural position, points to their formation later and at lower temperatures than awaruite.

Significantly less data is available for the awaruite of Karaginsky island due to the lack of material. The few grains available show intergrowths with serpentine and sulfide inclusions that are less common than awaruite from other localities.

Awaruite from rivers related to the Mamet ophiolite is similarly defined by complex mineralogy and structure. It often comprises inclusions of andradite and magnetite (Figure 4(a)) and forms replacement rims around pentlandite (Figure 4(b)). In contrast to Kamchatsky Mys, wairauite from the Mamet complex is abundant and occurs as fine-grained rims surrounding silicate inclusions in awaruite (Figure 4(f)). Larger, euhedral wairauite grains (Figures 2(e) and 2(f)) may host disseminated garnet (andradite) inclusions (Figures 4(g) and 4(h)) or appear homogeneous with simple inner structures (Figure 4(i)).

4.3. Characteristics of Awaruite from the Galmoenan Complex Placers. Awaruite from placers related to the Galmoenan complex has already been extensively described by Sidorov et al. [19]. In serpentinized dunite, it occurs within serpentine veinlets or forms alteration rims after pentlandite. Awaruite is often accompanied by wairauite, heazlewoodite Ni_3S_2, millerite NiS, orcelite ($Ni_{5-x}As_2$ where $x \sim 0.25$), maucherite $Ni_{11}As_8$, and other BMS and arsenides. Both awaruite and wairauite form intergrowths with isoferroplatinum, sperrylite, and an unnamed Pd-Sb phase [19].

4.4. PGMs and Gold Inclusions in Awaruite of Kamchatsky Mys. Awaruite from Kamchatsky Mys comprises numerous minute inclusions of PGM (Figure 5), which, due to their size, were only able to be analyzed qualitatively via EDS. They can be subdivided into three groups: Os-Ir-Ru phases (Figures 5(a)–5(c)), Pt-dominant phases (Figures 5(d)–5(f)), and Pd-dominant phases (Figures 5(g) and 5(h)). Platinum-dominant phases do not contain any measurable Os, Ir, or Ru and vice versa. Moreover, they often contain Cu and elevated Fe relative to the awaruite matrix, whereas

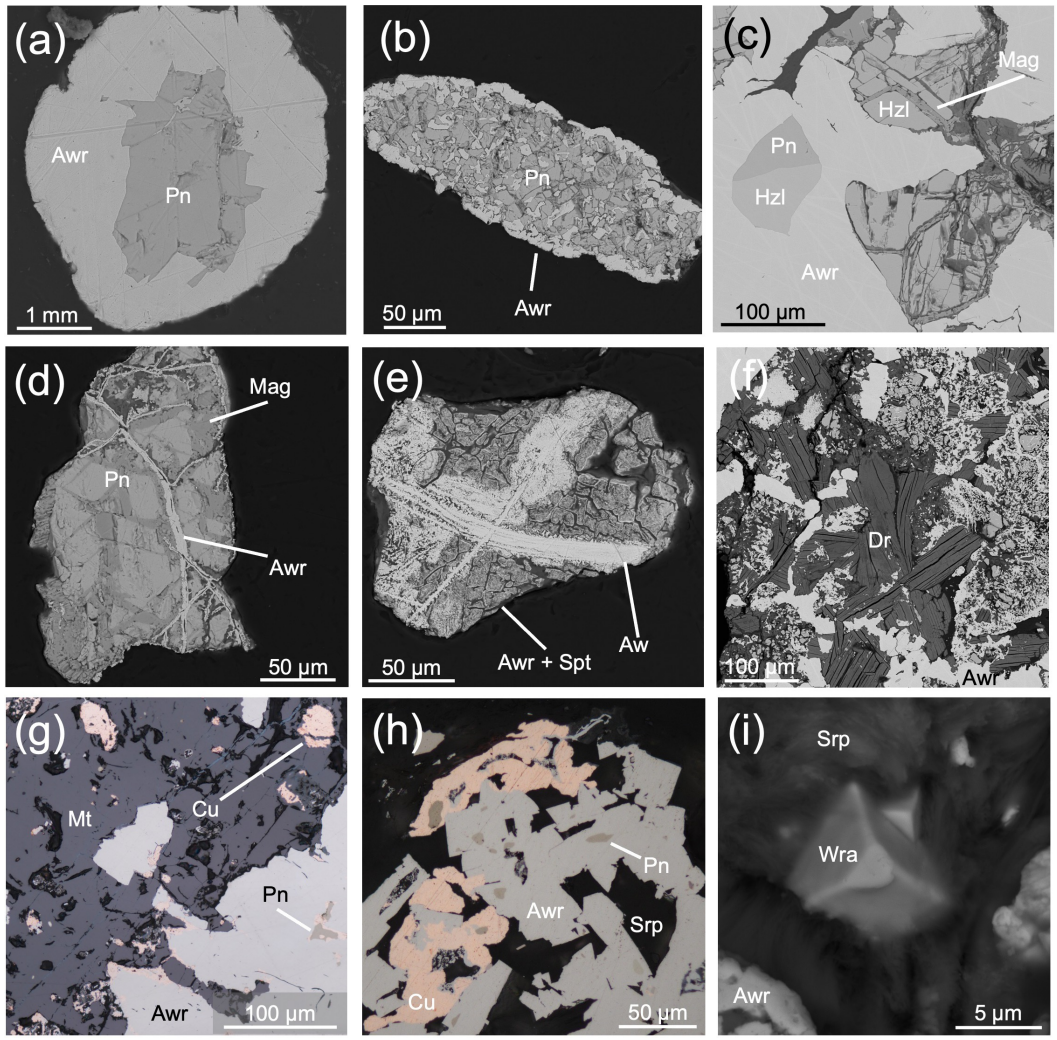

FIGURE 3: BSE (a–f and i) and reflected light microscopy (g and h) images of Kamchatsky Mys awaruite grains. (a) Internal structure of awaruite grain revealing the core of pentlandite; (b) pentlandite grain with a rim of awaruite; (c) awaruite with inclusions of pentlandite and heazlewoodite, the latter is altered by magnetite; (d) pentlandite with veinlets of awaruite and magnetite; (e) awaruite-serpentine aggregate with veinlets of pure awaruite; (f) droninoite inclusions in awaruite; (g and h) native copper occupying interstitial space in awaruite-magneite aggregate and altering awaruite; (i) wairauite in serpentine. Mineral abbreviations: Awr – awaruite, Pn – pentlandite, Hzl – heazlewoodite, Mag – magnetite, Srp – serpentine, Cu – native copper, Dr – droninoite, and Wra – wairauite.

Os-Ir-Ru phases lack Cu. Therefore, it is very plausible that Pt-dominant phases are Pt-Fe-Cu alloys, such as tetraferroplatinum PtFe or tulameenite Pt_2CuFe, while Os-Ir-Ru phases similarly correspond to alloys. Ferronickelplatinum Pt_2FeNi was also identified (Figure 5(f)). Palladium phases occasionally occur as grains large enough for EDS analysis (Figures 5(g) and 5(h)). These are defined by Pd:Sb ratios comparable to naldrettite (Pd_2Sb); however, they also contain ~10 wt.% Cu, which cannot be attributed to matrix interference and is therefore classified as an unnamed mineral. Native silver (≈Ag_3Au) and auricupride (Cu_3Au) were observed as rims around the awaruite (Figure 5(i)).

4.5. Major and Minor Element Chemistry of Awaruite, Wairauite, and Sulfides. Awaruite from all localities is relatively stoichiometric in composition with some variation in minor components (Figure 6). Average Co content is ~0.4 wt.% for Kamchatsky Mys, 0.6 wt.% for Karaginsky, and 1.1 wt.% for Mamet. The latter also shows the highest scatter: from 0.35 to 4.0 wt.% Co. Galmoenan awaruite contains the most Co (~1.2 wt.%) with low variability (0.5 and 1.9 wt.%). Sulfides from Mamet are Co-rich (up to 15 wt.% in pentlandite), whereas sulfides from Galmoenan typically contain <2 wt.% Co. Copper content of awaruite varies significantly from 0.02 to 2.7 wt.% in all localities. Sulfides from ophiolitic samples typically contain negligible Cu (below detection limits [b.d.l.] to 0.04 wt.%), whereas pentlandite from Galmoenan contains up to 1.3 wt.% Cu (Supplementary Table S1).

4.6. PGE and Au Content in Awaruite and Pentlandite. PGEs and Au were analyzed in awaruite, pentlandite, wairauite, and magnetite, but the latter two were consistently b.d.l.; the results are represented in Figure 7.

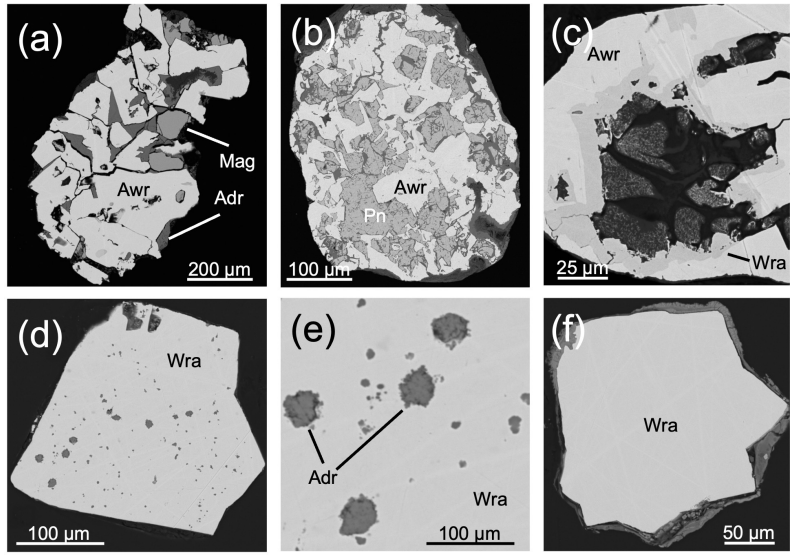

Figure 4: BSE images of the internal structure of awaruite (a–c) and wairauite (d–f) grains from placers related to the Mamet ophiolite. (a) Andradite and magnetite intergrowing with awaruite; (b) awaruite with relicts of pentlandite; (c) wairauite rim around awaruite; (d and e) wairauite with andradite inclusions; (f) twinned wairauite crystal. Mineral abbreviations: Adr – andradite.

Several analyses of Galmoenan awaruite yielded high Os content; however, downhole time-resolved spectra reveal an inhomogeneous Os distribution (Figure 8(a)). These irregular zones differ from the classical narrow spikes that are usually interpreted as microscale inclusions or "nuggets," whose size, given the volume of material ablated during the analysis, should be significantly smaller than the size of the beam (43 μm). Osmium enrichment correlates with sulfur (Figure 8(a)), indicating that inclusions of sulfides, presumably Os-rich pentlandite.

In ophiolitic complexes, Os does not exceed 0.1 ppb in awaruite (Mamet-line1 – 16; Table S1). Palladium content is strongly variable (Figure 7). Although most analyses were b.d.l., the highest concentrations were measured from the Galmoenan complex (up to 3 ppm); few samples with Pd content of ≈0.1 ppm were observed in Karaginsky and Kamchatsky Mys. High Pd samples are not enriched in Os or any other PGE. Gold content is highest in awaruite from Karaginsky island (1 ppm max., average 0.4, n = 11) and shows the homogeneous distribution in downhole time-resolved spectra (Figure 8(e)). Awaruite from other localities contains much less gold: up to 0.26 ppm in Mamet and 0.15 ppm in Kamchatsky Mys and Galmoenan.

Sulfides from the Galmoenan complex often show extremely high Os contents (up to 540 ppm). In this case, Os spectra are very smooth, indicating a homogeneous Os distribution. This suggests that Os may be incorporated in the pentlandite lattice; however, this has not been reported previously in the literature. One analysis of pentlandite from the Galmoenan complex yielded 300 ppm Os, 1.1 ppm Ir, 1.0 ppm Ru, 0.1 ppm Rh, 1.7 ppm Pt, and 0.1 ppm Pd (Figure 8(c)). In other complexes, Os is typically b.d.l. in pentlandite. Palladium is low, normally approaching the detection limits. The gold content is low (up to 40 ppb, usually b.d.l.) in all analyzed pentlandite grains.

5. Discussion

5.1. Formation Mechanism of Awaruite-Sulfide Associations. Given that terrestrial awaruite has only been found in serpentinized peridotites and related placers [17], and all the samples studied were collected in the vicinity of peridotites, we can assume that dunite, harzburgite, and other rocks of these complexes are the primary metal source for the placer grains studied (Figure 1). As olivine is replaced during serpentinization, Ni^{2+} in olivine is reduced, whereas Fe^{2+} disproportionates to Fe^0 and Fe^{3+}, forming magnetite, serpentine, and awaruite, represented by the following unbalanced reaction:

$$4(Mg,Fe,Ni)_2SiO_4 + 2H_2O \leftrightarrow 2Mg_3Si_2O_5(OH)_4 + FeFe_2O_4 + Ni_3Fe + H_2 \quad (1)$$

This process suggests the formation of awaruite as a result of olivine breakdown [13], which is supported by textural evidence in many ultramafic complexes [17, 51]. However, our observations also indicate that awaruite forms on behalf of pentlandite, occurring as rims (Figures 3(a), 3(b), and 4(b)) and veinlets associated with magnetite (Figure 3(d)). This can be described by the following reaction:

$$(Fe,Ni)_9S_{8(Pentlandite)} + 8H_2O_{(aq)} \leftrightarrow 8\ H2S_{(aq)} + 3Ni_3Fe_{(Awaruite)} + 2Fe_3O_{4(Magnetite)} \quad (2)$$

Such redox processes may also involve Cr-spinel, which has shown elevated Fe in reaction rims (forming Cr-magnetite) near the contact with awaruite [21], which likely sourced Fe_2O_3 during the breakdown of olivine.

5.2. Factors Controlling PGE Budget of Awaruite. Our study of awaruite from placers related to the Kamchatsky Mys, Karaginksy Island, and Mamet ophiolitic peridotites demonstrates negligible contents of PGE, typically b.d.l. (Figure 7). This is similar to PGE-depleted awaruite from

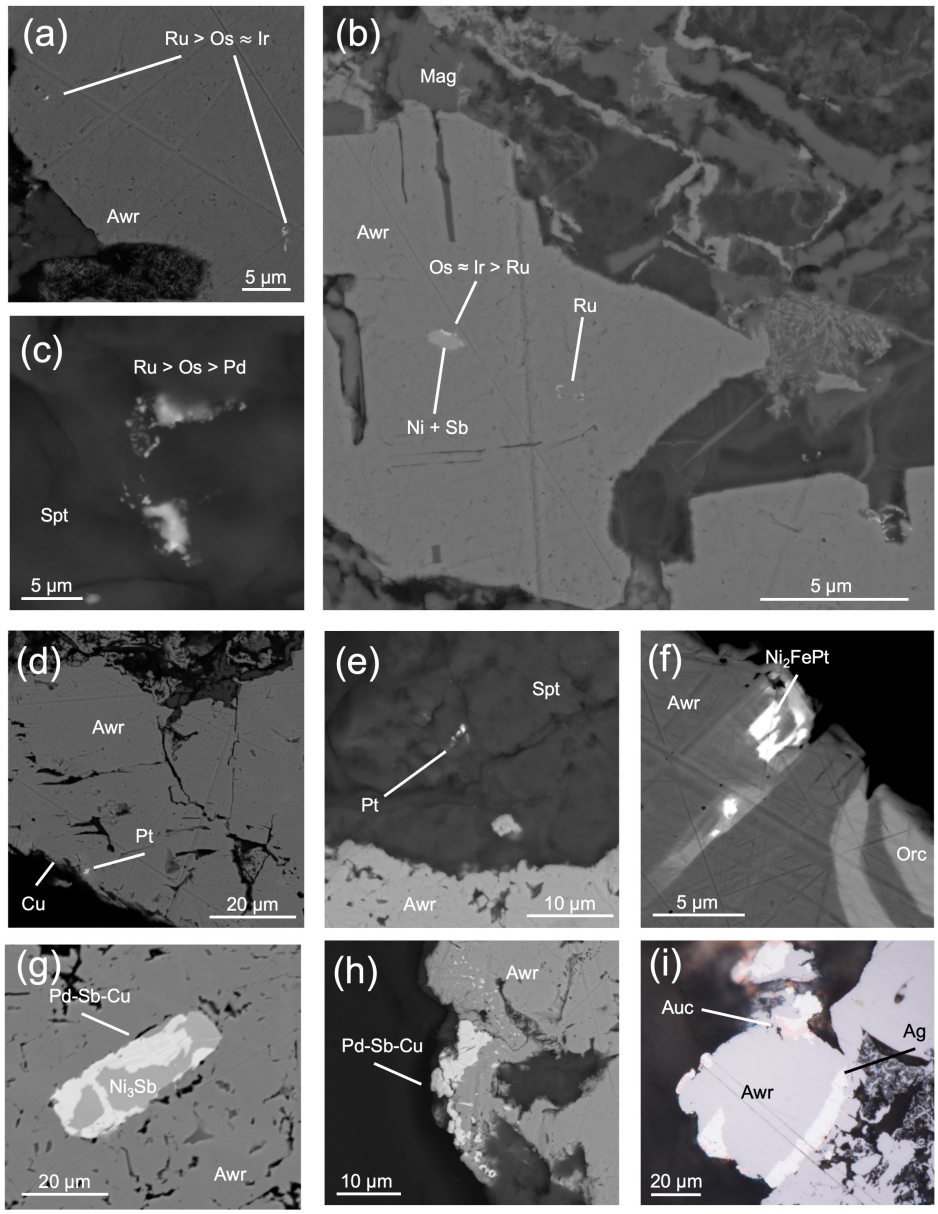

Figure 5: BSE (a–h) and reflected light microscopy (i) images of PGM and gold associated with awaruite from Kamchatsky Mys ophiolite. (a and b) Inclusions of Os-Ir-Ru alloys in awaruite; (c) Ru-rich alloy in serpentine; (d) Pt-rich phase in native copper rim after awaruite; (e) Pt-rich phase in serpentine; (f) Ni_2FePt and orcelite ($Ni_{5-x}As_2$ where $x \sim 0.25$) inclusion in awaruite; (g) inclusion of Pd-Sb-Cu and Ni_3Sb in awaruite; (h) Pd-Sb-Cu rims and symplectites with awaruite; (i) gold-rich native silver and auricupride rim on awaruite. Mineral abbreviations: Orc – orcelite, Taur – tetraauricupride, and Ag – native silver.

the La Cabana ophiolite (Table 1; Reference [23]); however, it is in contrast to moderate-to-high PGE abundances reported in awaruite from the Nahlin ophiolite [22]. Direct comparison of awaruite, reported in different studies, is thus influenced by the mode of PGE occurrence, such as PGE in solid solution and/or the presence and distribution of minute PGM nuggets. The importance of both factors is hard to evaluate at present, given the extremely limited number of published LA-ICP-MS analyses (sixteen in total). Nevertheless, exceptionally low PGE abundances in awaruite are unexpected and require explanation. The PGE budget in awaruite that forms during hydrothermal alteration (serpentinization) of host peridotite rocks principally depends on PGE availability prior to alteration, PGE behavior in hydrothermal fluids, and secondary PGM that may remobilize PGE during awaruite formation (Figure 9).

5.2.1. Potential Sources of PGE Among Precursor Minerals. There are two main potential sources of PGE in host peridotites prior to and during serpentinization: Cr-spinel and PGE-rich minerals, such as BMSs and PGM. In general, the Cr-spinel phenocrysts in volcanic rocks contain tens of ppb IPGE (iridium-group PGE = Os, Ir, and Ru) and Rh in solid solution but are free of Pt and Pd [52–54]. Additionally, PGM nuggets, ranging from sub-μm to several

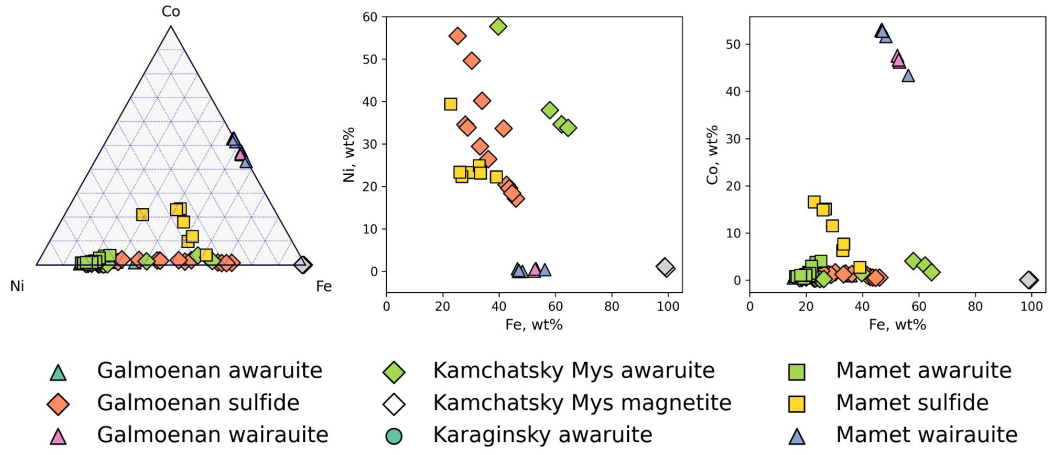

FIGURE 6: Major element contents of awaruite, wairauite, and sulfides (measured by LA-ICP-MS).

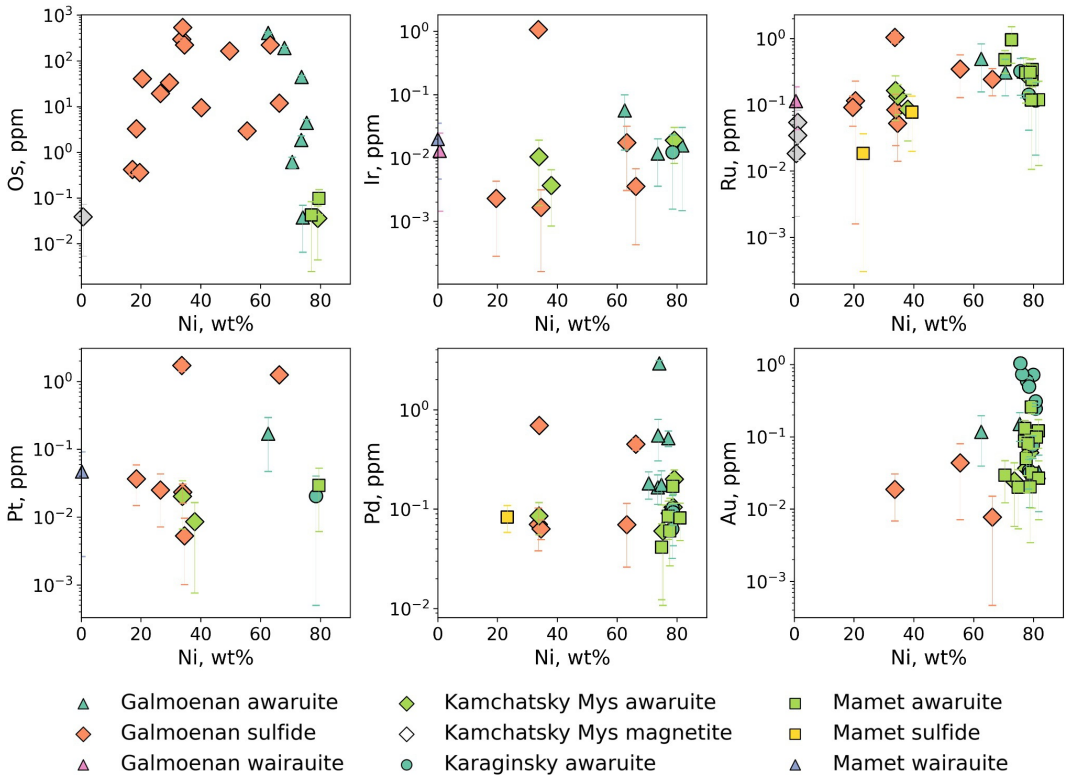

FIGURE 7: LA-ICP-MS data of PGE and Au in awaruite and pentlandite. (a) Ni versus Os, (b) Ni versus Ir, (c) Ni versus Ru, (d) Ni versus Pt, (e) Ni versus Pd, and (f) Ni versus Au. Samples with precious metal content b.d.l. or less than 1σ are not shown.

μm in size, contain all PGE aside from Pd and commonly occur within Cr-spinel in volcanic rocks and chromitites in dunites [53–56]. Although being a relatively robust phase during alteration, Cr-spinel can be partially or fully replaced by secondary minerals (e.g., magnetite and stichtite) and dissolved into serpentinizing fluids, resulting in the release of PGE and PGM contained in Cr-spinel.

Sulfides are the other potential source of PGE. High silicate/sulfide partitioning coefficients make it almost inevitable for magmatic sulfides to contain measurable amounts of PGE [57]. In abyssal peridotites from Mid-Atlantic and South West Indian ridges, the average PGE content of pentlandite is 5.9 ppm Os, 5.6 ppm Ir, 6.9 ppm Ru, 0.54 ppm Rh, 0.08 ppm Pt, and 1.9 ppm Pd [58]. Sulfide globules from primitive lavas of the Kamchatsky Mys ophiolite yielded lower IPGE and Rh but higher Pt and Pd contents (up to 7.03 ppm Pt and 4.40 ppm Pd [59]). Sulfides from the Nahlin ophiolite also comprise significant PGE [22]. Being susceptible to the alteration, sulfides likely release PGE during serpentinization.

The other possible PGE sources are primary PGM. Ophiolitic peridotites are characterized by a diverse assemblage of PGM that is dominated by laurite $(Ru,Os)S_2$, Os-Ir-Ru alloys, and Pt-Fe alloys [60, 61]. The Olkho-

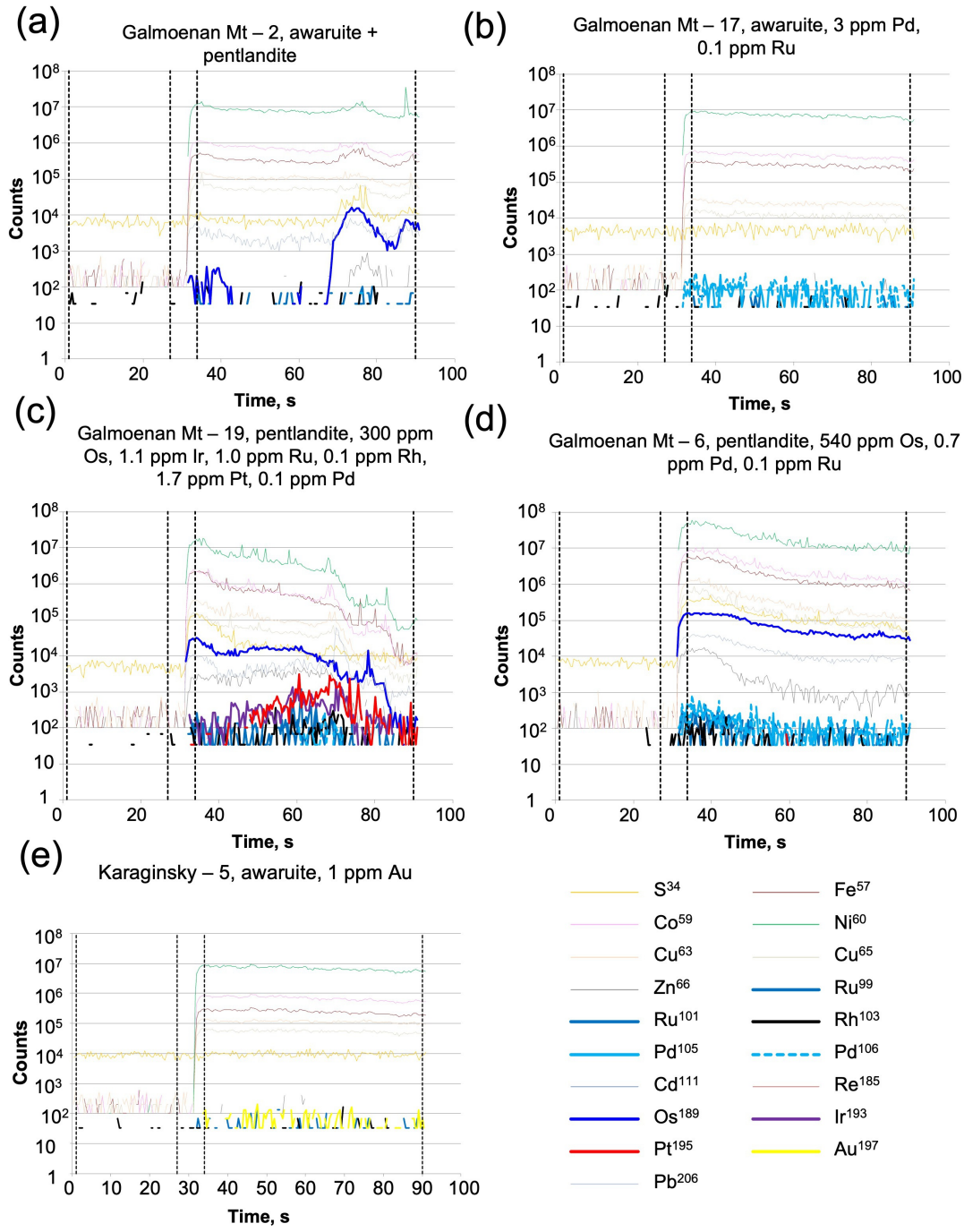

Figure 8: Selected downhole time-resolved spectra of LA-ICP-MS spot analysis of pentlandite and awaruite from Galmoenan (a–d) and Karaginsky Island (e).

vaya-1 placer in the direct vicinity of the Kamchatsky Mys ophiolite comprises PGM assemblages containing 73% Os-Ru-Ir alloys, 25% of isoferroplatinum Pt_3Fe, and 3% of other minerals [34]. This implies that the source rocks of the studied awaruite most likely contain similar mineral assemblages. Although primary PGM is generally believed to be robust during the hydrothermal stage, their alteration is not uncommon [34, 62–65], thus they may also be an important source of PGE in hydrothermal fluids.

5.2.2. PGE Behavior in Hydrothermal Fluids. The mobility of PGE in hydrothermal fluids strongly determines whether PGE-bearing phases can form from precursor minerals. Ballhaus and Stumpfl [66] attributed the formation of large PGM on the outer parts of sulfide grains in the Merensky Reef to the transportation of PGE as Cl^- complexes in saline fluids. Subsequent experimental work showed that Pt may be highly mobile in a fluid phase [67]. More recent studies

Table 1: Summary of reported PGE admixtures and PGM inclusions in awaruite here and elsewhere.

	Ophiolitic peridotite		Ural-Alaskan type	
Admixtures of PGE and Au in awaruite				
Os	Up to 23.64 ppm, Nahlin ophiolite	[22]	**Up to 89.1 ppm (likely due to the inclusions of Os-bearing pentlandite), Galmoenan complex**	This study
Ir	Up to 6.74 ppm, Nahlin ophiolite	[22]	**Up to 0.08 ppm, single analysis, Galmoenan complex**	This study
Ru	–			
Rh	Up to 6.9 ppm, La Cabana	[23]	–	
Pt	–			
Pd	Up to 19.85 ppm, Nahlin ophiolite; up to 2.5 ppm, La Cabana ophiolite	[22, 23]	**Up to 3 ppm, Galmoenan complex**	This study
Au	Up to 1.04 ppm, Karaginsky ophiolite		–	
Inclusions of PGM in awaruite				
Pt-Fe alloys	**Pt-Fe-Ni alloys, including ferronickelplatinum and unnamed Ni_2FePt phase, Kamchatsky Mys ophiolite**	This study	Various Pt-Fe alloys, Galmoenan complex; tomamaeite Cu_3Pt, isoferroplatinum Pt_3Fe, tulameenite Pt_2FeCu ferronickelplatinum Pt_2FeNi, Matysken complex.	[19, 20]
Os-Ir-Ru alloys	**Os-Ir-Ru alloys (various proportions, possibly – hexaferrum and related Os-Ir-Ru-Fe-[Ni] phases), Kamchatsky Mys ophiolite;** "Iridian awaruite" (up to 27 wt.% Ir), Ru-Os-Ir-Ni-Fe alloy (hexaferrum?), and Sakhakot-Chila ophiolite	This study	**Inclusions of Os-rich pentlandite, Galmoenan complex**	This study
Sb-bearing phases	**Pd-Sb-Cu phases and Kamchatsky Mys ophiolite**	This study	Bi-Pd phases, Matysken complex	[20]
As-bearing phases	–		Irarsite, Ir-As-S, Matysken complex	[20]
Au-Ag minerals	**Au-rich native silver, auricupride Cu_3Au, and Kamchatsky Mys ophiolite**	This study	Native silver, Au-Ag-Te phases, Galmoenan complex	
Other minerals	–		Bi-Pd phases, Galmoenan complex	[20]

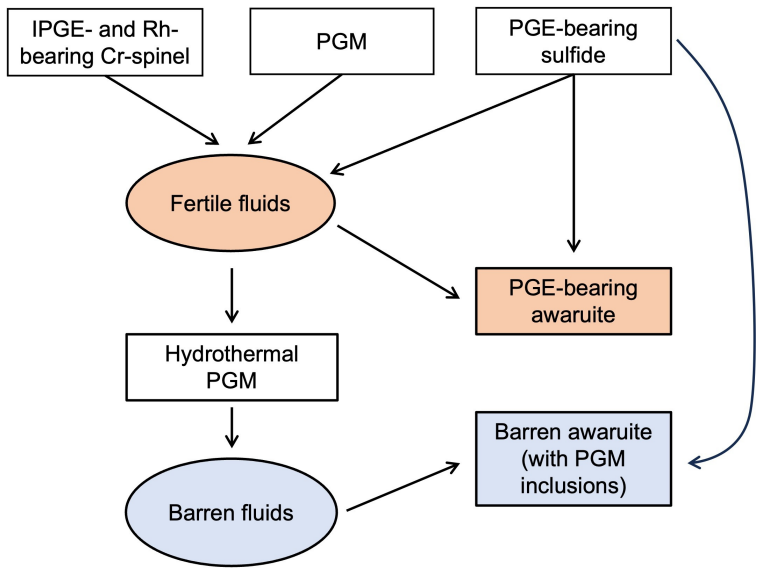

Figure 9: Potential formation mechanisms for PGE-rich and PGE-barren awaruite during serpentinization.

support these findings, with particular emphasis on the role of bisulfide complexes in the transport of Pd and Pt [68].

Unlike Pd and Pt, IPGE is often considered immobile during hydrothermal alteration [69]. However, this point of view is currently challenged by studies of Os oxide crystallization from hydrothermal fluids [70] and Os and Ir mobility in oxidized fluids in upper mantle/lower crustal conditions [71]. In addition, there is significant textural evidence that at least some Os-, Ir-, and Ru-based alloys may form during the hydrothermal alteration of laurite and primary alloys [63, 72].

5.2.3. Partitioning of PGE in Awaruite-Bearing Mineral Assemblages. Three groups of PGM have been found in association with awaruite from ophiolitic peridotites (Table 1): (1) Pt-Fe-(Cu) alloys (Figures 5(d)–5(f)), (2) Pd-Sb minerals (Figures 5(g) and 5(h)), and (3) Os-Ir-Ru alloys (Figures 5(a)–5(c)).

According to previous studies, some Pt-Fe alloys may be of hydrothermal origin. Tetraferroplatinum, ferronickelplatinum, and tulameenite are systematically reported in serpentine veins from chromitites of Ural-Alaskan type complexes or as rims over primary Pt-Fe alloys, such as isoferroplatinum [4, 64]. In some cases, isoferroplatinum is subsequently replaced by tetraferroplatinum, unnamed Fe_3Pt ± native iron [56]. Taken together with the experimental data on Pt mobility in hydrothermal solutions, this suggests a hydrothermal origin for Pt-Fe-(Cu) alloys.

Abundant Pt alloy and Pd mineral inclusions in awaruite (Figures 5(g) and 5(h)) are likely of hydrothermal origin, which has been inferred for similar phases in serpentinized peridotites elsewhere [73]. This is supported by textural observations, that is, they form intimate intergrowths with awaruite (Figure 5(h)) that indicate their coeval crystallization or replacement of awaruite. Although they are spatially related to awaruite and serpentine, we cannot be certain of the hydrothermal origin of Os-Ir-Ru alloys here (Figures 5(a)–5(c)).

The abundance of secondary PGM inclusions can thus explain the low PGE measured in awaruite here. It appears that PGE was mobilized during hydrothermal alteration and preferentially partitioned to these phases rather than awaruite in this case. An additional explanation, and likely more prominent here, for low PGE in awaruite is the fact that it formed on behalf of PGE-barren pentlandite, which is in contrast to the PGE-rich awaruite analyzed from the Nahlin ophiolite.

5.3. Awaruite and Osmium-Rich Pentlandite of the Galmoenan Complex. In the Galmoenan complex, the principal formation mechanism of awaruite is similar to those described for ophiolitic peridotites; hence, the same source–mobility–secondary PGM logic may be applied.

Several pentlandite inclusions in awaruite contain anomalously high, previously unreported, Os (up to 540 ppm; Figure 8(d)) but show no enrichment in other PGE. This provides additional evidence for the nonmagmatic origin of such pentlandite because known partitioning coefficients between pentlandite, pyrrhotite, and other sulfides [57, 74] do not allow for the preferential enrichment of pentlandite in osmium during magmatic processes. Moreover, Pd content of magmas that are considered to be parental for Ural-Alaskan type complexes is more than an order of magnitude higher than Os [75].

Awaruite that replaces pentlandite (either Os-rich or regular PGE-barren) does not contain any significant PGE with the exception of three Pd-bearing grains (Figure 3(c)). This implies that Os does not partition to awaruite during alteration here, although awaruite has the capacity to concentrate Pd.

6. Conclusions

(1) Awaruite formed via desulfurization of pentlandite during serpentinization. No significant PGE concentrations have been measured in awaruite from the Kamchatsky Mys, Karaginsky Island, or Mamet ophiolites, in contrast to previous studies on awaruite from other ophiolitic ultramafics. Few analyses of awaruite from the Galmoenan complex yielded significant PGE (up to 3 ppm Pd). To resolve the contradiction with previously published data, a multiplicity of factors that control the PGE budget of awaruite should be considered. They include, but are not limited to, the PGE content in precursor minerals (Cr-spinel, sulfide, or PGM), PGE mobility in hydrothermal fluids, and secondary PGM that coprecipitate with awaruite and are able to fractionate PGE. Out of these, our study suggests that the main factor that controls PGE content of awaruite is the PGE abundance of precursor sulfide.

(2) Three groups of PGM are associated with awaruite from Kamchatsky Mys. The most common are minute Pt-Fe alloys that likely correspond to ferronickelplatinum (Pt_2FeNi) or unnamed Ni_2FePt alloys, which have been reported as products of isoferroplatinum alteration during serpentinization in ultramafic complexes elsewhere. Osmium-Ir-Ru inclusions also occur within awaruite, but there is no irrefutable evidence for their secondary origin. The other group of inclusions found in awaruite is Pd antimonides, which formed simultaneously with awaruite and serpentine during hydrothermal alteration.

(3) Some pentlandite grains from placers related to the Galmoenan Ural-Alaskan type complex yield exceptionally high, previously unreported, Os content (up to 540 ppm). Such anomalies are not accompanied by elevated Ir or Ru, indicating selective enrichment of Os. Considering known silicate/sulfide partitioning coefficients for PGE, compositions of parental melts for Ural-Alaskan type complexes, and the textural position of pentlandite, such anomalous Os contents cannot have formed as a result of a magmatic process. This

implies Os mobility during dunite alteration. Awaruite replacing this pentlandite does not contain anomalous Os.

Conflicts of Interest

The authors declare that they have no conflicts of interest.

Acknowledgments

The paper was partly based on samples from the collection of Evgeniy Sidorov (1955-2021) whom we want to commemorate. We are grateful to Valeria D. Brovchenko for critical remarks and assistance with processing LA-ICP-MS analyses. Associate Editor Aleksandr S. Stepanov and two anonymous reviewers are warmly acknowledged for their constructive remarks. This investigation was partly (TY) supported Ministry of Science and Higher Education of the Russian Federation project [FSWW-2023-0010]and the Visiting Scientist Award by the Chinese Academy of Sciences (VSK).

Supplementary Materials

Supplementary material available: the results of LA-ICP-MS analyses, detection limits, and uncertainties. All technical details are provided in Methods. Additional data and materials, including awaruite samples, are available upon request.

References

[1] A. Naldrett, "Fundamentals of Magmatic sulfide deposits," in *Magmatic Ni-Cu and PGE Deposits: Geology, Geochemistry, and Genesis*, C. Li, and E.M. Ripley, Eds., Society of Economic Geologists, 2011.

[2] J. E. Mungall and A. J. Naldrett, "Ore deposits of the platinum-group elements," *Elements*, vol. 4, no. 4, pp. 253–258, 2008.

[3] J. Thakurta, "Alaskan-type complexes and their associations with economic mineral deposits," in *Processes and ore deposits of ultramafic-mafic magmas through space and time*, pp. 269–302, Elsevier Inc, 2018.

[4] L. J. Cabri, T. Oberthür, and R. R. Keays, "Origin and Depositional history of platinum-group minerals in Placers – A critical review of facts and fiction," *Ore Geology Reviews*, vol. 144, p. 104733, 2022.

[5] D. C. Peck, R. R. Keays, and R. J. Ford, "Direct crystallization of refractory platinum-group element alloys from Boninitic Magmas: Evidence from Western Tasmania," *Australian Journal of Earth Sciences*, vol. 39, no. 3, pp. 373–387, 1992.

[6] J. Farré-de-Pablo, J. A. Proenza, J. M. González-Jiménez, et al., "Low-temperature Hydrothermal PT mineralization in Uvarovite-bearing Ophiolitic Chromitites from the Dominican Republic," *Mineralium Deposita*, vol. 57, no. 6, pp. 955–976, 2022.

[7] G. Garuti, E. Pushkarev, O. A. R. Thalhammer, and F. Zaccarini, "Chromitites of the Urals (part 1): Overview of chromite mineral chemistry and Geotectonic setting," *Ofioliti*, vol. 37, pp. 27–53, 2012.

[8] R. R. Keays, D. A. Holwell, and H. M. Prichard, "Platinum Mineralisation in the Owendale Uralian-Alaskan-type complex, New South Wales, Australia: the effects of Serpentinization on cu-PGE-NI Sulphides," *Ore Geology Reviews*, vol. 130, p. 103928, 2021.

[9] K. A. Evans, B. R. Frost, S. M. Reddy, and T. C. Brown, "Causes, effects, and implications of the relationships amongst fluids, Serpentinisation, and alloys," *Lithos*, vols. 446–447, p. 107132, 2023.

[10] G. L. Früh-Green, A. D. James, A. Plas, D. S. Kelley, and G. Bernard, *"Serpentinization of Oceanic Peridotites: Implications for Geochemical Cycles and Biological Activity,"* Vol. 144, 2004.

[11] B. W. Evans, K. Hattori, and A. Baronnet, "Serpentinite: What, why, where," *Elements*, vol. 9, no. 2, pp. 99–106, 2013.

[12] K. A. Evans, S. M. Reddy, A. G. Tomkins, R. J. Crossley, and B. R. Frost, "Effects of Geodynamic setting on the redox state of fluids released by Subducted Mantle Lithosphere," *Lithos*, vols. 278–281, pp. 26–42, 2017.

[13] F. Klein and W. Bach, "Fe-NI-Co-O-S phase relations in Peridotite-seawater interactions," *Journal of Petrology*, vol. 50, no. 1, pp. 37–59, 2009.

[14] D. I. Foustoukos, M. Bizimis, C. Frisby, and S. B. Shirey, "Redox controls on NI–Fe–PGE mineralization and re/os fractionation during Serpentinization of Abyssal Peridotite," *Geochimica et Cosmochimica Acta*, vol. 150, pp. 11–25, 2015.

[15] R. I. Botto and G. H. Morrison, "Josephinite; a unique nickel-iron," *American Journal of Science*, vol. 276, no. 3, pp. 241–274, 1976.

[16] A. Peretti, J. Dubessy, J. Mullis, B. R. Frost, and V. Trommsdorff, "Highly reducing conditions during Alpine Metamorphism of the Malenco Peridotite (Sondrio, northern Italy) indicated by mineral Paragenesis and H2 in fluid inclusions," *Contributions to Mineralogy and Petrology*, vol. 112, nos. 2–3, pp. 329–340, 1992.

[17] R. Britten, "Regional Metallogeny and genesis of a new deposit type-disseminated Awaruite (Ni_3Fe) mineralization hosted in the cache Creek Terrane," *Economic Geology*, vol. 112, no. 3, pp. 517–550, 2017.

[18] R. L. Brathwaite, A. B. Christie, and R. Jongens, "Chromite, platinum group elements and nickel Mineralisation in relation to the Tectonic evolution of the dun mountain Ophiolite belt, East Nelson, New Zealand," *New Zealand Journal of Geology and Geophysics*, vol. 60, no. 3, pp. 255–269, 2017.

[19] E. G. Sidorov., I. N. Sandimirova, V. M. Chubarov, and V. V. Ananev, "Accessory minerals of the Mafic-Ultramafic Massif Galmoenan (Koryakskoye upland, Kamchatka)," *Zapiski RMO (Proceedings of the Russian Mineralogical Society)*, vol. 147, no. 2, pp. 44–64, 2018. http://www.minsoc.ru/magazins.php?id=34&mid=21472.

[20] A. V. Kutyrev, E. G. Sidorov, V. S. Kamenetsky, V. M. Chubarov, I. F. Chayka, and A. Abersteiner, "Platinum mineralization and geochemistry of the Matysken zoned Ural-Alaskan type complex and related Placer (Far East Russia)," *Ore Geology Reviews*, vol. 130 p. 103947, 2021.

[21] T. Augé, L. J. Cabri, O. Legendre, G. McMahon, and A. Cocherie, "PGE distribution in base-metal alloys and

Sulfides of the new Caledonia Ophiolite," *The Canadian Mineralogist*, vol. 37, no. 5, pp. 1147–1161, 1999.

[22] C. J. M. Lawley, D. C. Petts, S. E. Jackson, et al., "Precious metal mobility during Serpentinization and breakdown of base metal sulphide," *Lithos*, vols. 354–355 p. 105278, 2020.

[23] J. M. González-Jiménez, R. Piña, J. E. Saunders, et al., "Trace element fingerprints of NI–Fe–S–as minerals in Subduction channel Serpentinites," *Lithos*, vols. 400–401 p. 106432, 2021.

[24] P. W. Scott, T. A. Jackson, and A. C. Dunham, "Economic potential of the Ultramafic rocks of Jamaica and Tobago: two contrasting geological settings in the Caribbean," *Mineralium Deposita*, vol. 34, no. 7, pp. 718–723, 1999.

[25] D. P. Savelyev, V. S. Kamenetsky, L. V. Danyushevsky, et al., "Immiscible sulfide melts in primitive Oceanic Magmas: Evidence and implications from Picrite Lavas (Eastern Kamchatka, Russia)," *American Mineralogist*, vol. 103, no. 6, pp. 886–898, 2018.

[26] N. V. Tsukanov, W. Kramer, S. G. Skolotnev, M. V. Luchitskaya, and W. Seifert, "Ophiolites of the Eastern peninsulas zone (Eastern Kamchatka): Age, composition, and Geodynamic diversity," *Island Arc*, vol. 16, no. 3, pp. 431–456, 2007. http://www.blackwell-synergy.com/toc/iar/16/3.

[27] M. Y. Khotin and M. N. Shapiro, "Ophiolites of the Kamchatsky Mys peninsula, Eastern Kamchatka: Structure, composition, and Geodynamic setting," *Geotectonics*, vol. 40, no. 4, pp. 297–320, 2006.

[28] A. B. Osipenko and K. A. Krylov, "Geochemical heterogeneity of Mantle Peridotites in the east Kamchatka Ophiolites: Causes and Geochemical implications," in *Petrology and Metallogeny of Mafic–Ultramafic Complexes of Kamchatka [in Russian]*, pp. 138–158, Nauchnyi Mir, 2001.

[29] M. E. Boyarinova, *Geological Map of Russia. Scale 1:200,000. East Kamchatka, Sheets O-58-KHKHVI, XXXI, XXXII. Explanatory Note [in Russian]*, Kartfabrika VSEGEI, 1999.

[30] V. P. Zinkevich, "Tectonics of the Kamchatsky Mys peninsula (East Kamchatka)," *Dokl Akad Nauk USSR*, vol. 285, no. 4, pp. 954–958, 1985.

[31] V. G. Batanova, Z. E. Lyaskovskaya, G. N. Savelieva, and A. V. Sobolev, "Peridotites from the Kamchatsky Mys: Evidence of Oceanic Mantle melting near a Hotspot," *Russian Geology and Geophysics*, vol. 55, no. 12, pp. 1395–1403, 2014.

[32] M. Portnyagin, K. Hoernle, and D. Savelyev, "Ultra-depleted melts from Kamchatkan Ophiolites: Evidence for the interaction of the Hawaiian plume with an Oceanic spreading center in the Cretaceous," *Earth and Planetary Science Letters*, vol. 287, nos. 1–2, pp. 194–204, 2009.

[33] M. Portnyagin, D. Savelyev, K. Hoernle, F. Hauff, and D. Garbe-Schönberg, "Mid-Cretaceous Hawaiian Tholeiites preserved in Kamchatka," *Geology*, vol. 36, no. 11, p. 903, 2008.

[34] N. Tolstykh, E. Sidorov, and A. Kozlov, "Platinum-group minerals from the Olkhovaya-1 Placers related to the Karaginsky Ophiolite complex, Kamchatskiy Mys peninsula, Russia," *The Canadian Mineralogist*, vol. 47, no. 5, pp. 1057–1074, 2009.

[35] S. G. Skolotnev, N. V. Tsukanov, and E. G. Sidorov, "New data on the composition of Ophiolite complexes on Karaginskii Island (Eastern Kamchatka)," *Doklady Earth Sciences*, vol. 479, no. 1, pp. 290–294, 2018.

[36] S. D. Sokolov, M. V. Luchitskaya, S. A. Silantyev, et al., "Ophiolites in accretionary complexes along the early cretaceous margin of NE asia: Age, composition, and geodynamic diversity," *Geological Society, London, Special Publications*, vol. 218, no. 1, pp. 619–664, 2003.

[37] V. G. Batanova, O. V. Astrakhantsev, and Ye. G. Sidorov, "The Dunites of the gal' Moenansk Pluton, Koryak Highlands," *International Geology Review*, vol. 33, no. 1, pp. 62–73, 1991.

[38] Y. V. Nazimova, V. P. Zaytsev, and S. V. Petrov, "The Galmoenan Massif, Kamchatka, Russia: Geology, PGE mineralization, applied Mineralogy and Beneficiation," *The Canadian Mineralogist*, vol. 49, no. 6, pp. 1433–1453, 2011.

[39] V. G. Batanova and O. V. Astrakhantsev, "Tectonic position and origins of the zoned Mafic-Ultramafic Plutons in the northern Olyutor zone, Koryak Highlands," *Geotectonics*, vol. 26, no. 2, pp. 153–165, 1992.

[40] V. G. Batanova, A. N. Pertsev, V. S. Kamenetsky, A. A. Ariskin, A. G. Mochalov, and A. V. Sobolev, "Crustal evolution of Island-arc Ultramafic Magma: Galmoenan Pyroxenite-Dunite plutonic complex, Koryak Highland (Far East Russia), " *Journal of Petrology*, vol. 46, no. 7, pp. 1345–1366, 2005.

[41] G. R. Himmelberg and R. A. Loney, "Characteristics and Petrogenesis of Alaskan-type Ultramafic-Mafic intrusions, southeastern Alaska," in *Professional Paper*, 1995.

[42] J. Košler. Edited by P. J. Sylvester, *Laser-Ablation ICPMS Study of Metamorphic Minerals and Processes, in Laser-Ablation in the Earth Sciences: Principles and Application*, Mineralogical Association of Canada, 2001.

[43] H. P. Longerich, S. E. Jackson, and D. Günther, "Inter-laboratory note. LASER ablation Inductively coupled plasma mass spectrometric transient signal data acquisition and Analyte concentration calculation," Journal of Analytical Atomic Spectrometry, vol. 11, no. 9, pp. 899–904, 1996.

[44] C. A. Norris, L. Danyushevsky, P. Olin, and N. R. West, "Elimination of Aliasing in LA-ICP-MS by alignment of laser and mass spectrometer," *Journal of Analytical Atomic Spectrometry*, vol. 36, no. 4, pp. 733–739, 2021.

[45] I. Belousov, L. Danyushevsky, K. Goemann, et al., "STDGL3, a reference material for analysis of sulfide minerals by laser ablation ICP-MS: An assessment of matrix effects and the impact of laser wavelengths and pulse widths," *Geostandards and Geoanalytical Research*, vol. 47, no. 3, pp. 493–508, 2023. https://onlinelibrary.wiley.com/toc/1751908x/47/3.

[46] S. Gilbert, L. Danyushevsky, P. Robinson, et al., "A comparative study of five reference materials and the Lombard meteorite for the determination of the platinum-group elements and gold by LA-ICP-MS," *Geostandards and Geoanalytical Research*, vol. 37, no. 1, pp. 51–64, 2013. http://doi.wiley.com/10.1111/ggr.2013.37.issue-1.

[47] P. Sylvester, "Laser ablation Inductively coupled mass spectrometer (LA ICP-MS)," in *Encyclopedia of scientific dating methods,* W. Jack Rink, and J.W. Thompson, Eds., Springer Netherlands: Dordrecht, 2015.

[48] L. Danyushevsky, P. Robinson, S. Gilbert, et al., "Routine quantitative multi-element analysis of sulphide minerals by laser ablation ICP-MS: Standard development and consideration of matrix effects," *Geochemistry*, vol. 11, no. 1, pp. 51–60, 2011.

[49] S. E. Gilbert, L. V. Danyushevsky, T. Rodemann, et al., "Optimisation of laser parameters for the analysis of sulphur Isotopes in sulphide minerals by laser ablation ICP-MS," Journal of Analytical Atomic Spectrometry, vol. 29, no. 6, pp. 1042–1051, 2014.

[50] P. J. Sylvester. Edited by P. J. Sylvester, *A Practical Guide to Platinum-Group Element Analysis of Sulphides by Laser-Ablation ICPMS, in Laser-Ablation in the Earth Sciences: Principles and Application*, Mineralogical Association of Canada, 2001.

[51] E. I. Sandimirova, E. G. Sidorov, and V. M. Chubarov, "Accessory iron and nickel minerals from the Mt. Poputnaya Ultramafic Massif, Eastern Kamchatka, Russia," *Geology of Ore Deposits*, vol. 58, no. 7, pp. 586–593, 2016.

[52] M. Locmelis, M. L. Fiorentini, S. J. Barnes, E. J. Hanski, and A. F. Kobussen, "Ruthenium in chromite as indicator for Magmatic sulfide liquid Equilibration in Mafic-Ultramafic systems," *Ore Geology Reviews*, vol. 97 pp. 152–170, 2018.

[53] M. Locmelis, N. J. Pearson, S. J. Barnes, and M. L. Fiorentini, "Ruthenium in Komatiitic chromite," *Geochimica et Cosmochimica Acta*, vol. 75, no. 13, pp. 3645–3661, 2011.

[54] J.-W. Park, V. Kamenetsky, I. Campbell, G. Park, E. Hanski, and E. Pushkarev, "Empirical constraints on partitioning of platinum group elements between Cr-Spinel and primitive terrestrial Magmas," *Geochimica et Cosmochimica Acta*, vol. 216 pp. 393–416, 2017.

[55] V. S. Kamenetsky, J.-W. Park, J. E. Mungall, et al., "Crystallization of platinum-group minerals from silicate melts: Evidence from Cr-Spinel-hosted inclusions in volcanic rocks," *Geology*, vol. 43, no. 10, pp. 903–906, 2015.

[56] E. Sidorov, A. Kutyrev, V. Chubarov, and E. Zhitova, "Platinum mineralization of the Epilchik Ural-Alaskan type zoned complex (Far East Russia)," *Mineralium Deposita*, vol. 56, no. 1, pp. 143–160, 2021.

[57] J. E. Mungall and J. M. Brenan, "Partitioning of platinum-group elements and au between sulfide liquid and Basalt and the origins of Mantle-crust fractionation of the Chalcophile elements," *Geochimica et Cosmochimica Acta*, vol. 125 pp. 265–289, 2014.

[58] A. Luguet, O. Alard, J. P. Lorand, N. J. Pearson, C. Ryan, and S. Y. O'Reilly, "Laser-ablation Microprobe (LAM)-ICPMS Unravels the highly Siderophile element geochemistry of the Oceanic Mantle," *Earth and Planetary Science Letters*, vol. 189, nos. 3–4, pp. 285–294, 2001.

[59] D. P. Savelyev, S. V. Palesskii, and M. V. Portnyagin, "The source of platinum group elements in Basalts of the Ophiolite complex of the Kamchatsky Mys peninsula (Eastern Kamchatka)," *Russian Geology and Geophysics*, vol. 59, no. 12, pp. 1592–1602, 2018.

[60] B. O'Driscoll and J. M. González-Jiménez, "Petrogenesis of the platinum-group minerals," *Reviews in Mineralogy and Geochemistry*, vol. 81, no. 1, pp. 489–578, 2016.

[61] F. Zaccarini, E. Pushkarev, G. Garuti, and I. Kazakov, "Platinum-group minerals and other accessory phases in chromite deposits of the Alapaevsk Ophiolite, central Urals, Russia," *Minerals*, vol. 6, no. 4, p. 108, 2016.

[62] L. J. Cabri and A. D. Genkin, "Re-examination of PT alloys from Lode and Placer deposits, Urals," *Canadian Mineralogist*, vol. 29, no. May, pp. 419–425, 1991.

[63] A. G. Mochalovet al, "Hexaferrum (Fe,Ru), (Fe,Os), (Fe,IR) - a new mineral," *Zapiski RMO (Proceedings of the Russian Mineralogical Society)*, vol. 127, no. 5, pp. 41–51, 1998.

[64] N. Tolstykh, A. Kozlov, and Y. Telegin, "Platinum mineralization of the Svetly BOR and Nizhny Tagil intrusions, Ural platinum belt," *Ore Geology Reviews*, vol. 67 pp. 234–243, 2015.

[65] N. D. Tolstykh, E. G. Sidorov, and A. P. Kozlov, "Platinum-group minerals in Lode and Placer Deposts associated with the Ural-Alaskan-type Gal'Moenan complex, Koryak–Kamchatka platinum belt, Russia," *The Canadian Mineralogist*, vol. 42, no. 2, pp. 619–630, 2004.

[66] C. G. Ballhaus and E. F. Stumpfl, "Sulfide and platinum mineralization in the Merensky Reef: Evidence from hydrous silicates and fluid inclusions," *Contributions to Mineralogy and Petrology*, vol. 94, no. 2, pp. 193–204, 1986.

[67] C. Ballhaus, C. G. Ryan, T. P. Mernagh, and D. H. Green, "The partitioning of Fe, NI, Cu, PT, and au between sulfide, metal, and fluid phases: A pilot study," *Geochimica et Cosmochimica Acta*, vol. 58, no. 2, pp. 811–826, 1994.

[68] S. J. Barnes and W. Liu, "Pt and Pd mobility in Hydrothermal fluids: Evidence from Komatiites and from thermodynamic Modelling," *Ore Geology Reviews*, vol. 44 pp. 49–58, 2012.

[69] D. A. Holwell, Z. Adeyemi, L. A. Ward, et al., "Low temperature alteration of Magmatic NI-Cu-PGE Sulfides as a source for Hydrothermal NI and PGE ores: A quantitative approach using automated mineralogy," *Ore Geology Reviews*, vol. 91 pp. 718–740, 2017.

[70] H. Yan, Z. Liu, J. Di, and X. Ding, "Crystal growth of Osmium(IV) dioxide in chlorine-bearing Hydrothermal fluids," *Minerals*, vol. 12, no. 9, p. 1092, 2022.

[71] D. I. Foustoukos, "Hydrothermal oxidation of Os," *Geochimica et Cosmochimica Acta*, vol. 255 pp. 237–246, 2019.

[72] I. Uysal, F. Zaccarini, M. B. B. Sadiklar, and G. Garuti, "Occurrence of rare Ru-Fe-Os-IR-oxide and associated platinum-group minerals (PGM) in the Chromitite of Muğla Ophiolite, SW-Turkey," *Neues Jahrbuch Für Mineralogie - Abhandlungen*, vol. 185, no. 3, pp. 323–333, 2009.

[73] J. P. Lorand, O. Alard, and A. Luguet, "Platinum-group element Micronuggets and Refertilization process in Lherz Orogenic Peridotite (Northeastern Pyrenees, France)," *Earth and Planetary Science Letters*, vol. 289, nos. 1–2, pp. 298–310, 2010.

[74] E. T. Mansur, S.-J. Barnes, and C. J. Duran, "An overview of Chalcophile element contents of Pyrrhotite, Pentlandite, Chalcopyrite, and Pyrite from Magmatic NI-cu-PGE sulfide deposits," *Mineralium Deposita*, vol. 56, no. 1, pp. 179–204, 2021.

[75] A. V. Kutyrev, V. S. Kamenetsky, J.-W. Park, et al., "Primitive high-K Intraoceanic arc Magmas of Eastern Kamchatka: implications for paleo-Pacific Tectonics and Magmatism in the Cretaceous," *Earth-Science Reviews*, vol. 220 p. 103703, 2021.

[76] D. P. Savelyev, "Plagioclase Picrites in the Kamchatsky Mys peninsula, Eastern Kamchatka," *Journal of Volcanology and Seismology*, vol. 8, no. 4, pp. 239–249, 2014.

[77] V. P. Pokhilainen and V. P. Vasilenko. Edited by A. F. Mikhailov, *State Geological Map of the USSR, 1: 200 000. List P-58-XX, XXI*, Leningrad, Kartfabrika VAGT, 1970.

[78] O. V. Astrakhantsev, V. G. Batanova, and A. S. Perfilyev, "Structure of the Galmoenan Dunite-Clinopyroxenite-Gabbro Massif (Southern Koryakia)," *Geotectonics*, vol. 25, no. 2, pp. 132–144, 1991.